

A. Hrubciak¹, O. Khyzhun², B. Ostafiychuk^{1,3}, V. Moklyak^{1,3}, Yu. Yavorskyi⁴,
R. Lisovsky^{1,3,5}, L. Keush⁶, B. Onyskiv⁷

Nanostructured Mesoporous γ -Fe₂O₃: a Novel Photocatalyst for Degradation of Organic Pollutants

¹Institute of Metal Physics, National Academy of Science, Kyiv, Ukraine, hrubyak_andrii@ukr.net

²Institute of Materials Science I.M. Frantsevich, Kyiv, Ukraine, khyzhun@ukr.net

³Vasyl Stefanyk Precarpathian National University, 57 Shevchenko str., 76018

Ivano-Frankivsk, Ukraine, hrubyak_andrii@ukr.net

⁴National Technical University of Ukraine "Igor Sikorsky Kyiv Polytechnic Institute", Kyiv, Ukraine, yar-yr@ukr.net

⁵Ivano-Frankivsk National Medical University, Ivano-Frankivsk, Ukraine, lesrom2000@gmail.com

⁶National Metallurgical Academy of Ukraine, Dnipro, Ukraine, linakeush@gmail.com

⁷Ivano-Frankivsk Scientific Research Forensic Center of the Ministry of Internal Affairs of Ukraine, Ivano-Frankivsk, Ukraine, onuskivb@gmail.com

The modified sol-gel synthesis technique was used to create of nanostructured maghemite (γ -Fe₂O₃). It has been shown that the molar concentration of the original precursors during synthesis affects on the average particle sizes, specific surface area, pore size distributions, optical and conductivity properties. The XPS method allowed to establish features of electronic structure of the synthesized materials. Optimal conditions for the synthesis of nanostructured maghemite with mesoporous structure were selected. The mechanism of electrical conductivity formation for synthesized mesoporous materials was established. The width of the band gap is determined and its dependence on the molar concentration of precursors is established. The positive correlation between the specific surface area of γ -Fe₂O₃ samples and photocatalytic activity was established - the photocatalytic activity of synthesized γ -Fe₂O₃ increase with growth of specific surface area of samples.

Keywords: nanostructured maghemite, mesoporous structure, conductivity, specific surface area, band gap, photocatalyst.

Received 3 February 2021; Accepted 25 February 2021.

Introduction

Nanostructured iron oxides using in various fields of modern science and medicine due to its unique physico-chemical properties, which are clearly manifested in the nanoscale state [1-4]. The efficiency of a functional material using in each sphere depends on phase compositions, particles sizes, porous structure, etc. These factors have vast influence onto physical and chemical properties of material. The improving of synthesis methods of nanodispersed γ -Fe₂O₃ open new opportunities to obtaining of novel materials.

In this context, lately, there have been increasing reports of the use of iron oxide as a heterogeneous photo-

catalyst for wastewater treatment. The heterogeneous photocatalyst of semiconductor nature as Fe₂O₃, with the oxidation/reduction processes on the surface, are one of the most promising materials for practical for use as a photocatalyst. The application of Fe₂O₃ are due to several reasons: it are more productive in practical use and own greater stability in oxidation/reducing processes than molecular catalysts. Until now, titanium dioxide was the most common and studied heterogeneous photocatalyst. Iron oxide has advantages over titanium dioxide it exhibits the same performance as TiO₂ but has a simpler and ecological synthesis process. In addition, TiO₂ exhibits photocatalytic properties only during the ultraviolet light action. Since the solar spectrum contains

no more than 7% of ultraviolet radiation, this fact is a disadvantage for the practical application of titanium dioxide as photocatalyst. Nanostructured Fe₂O₃ are more effective photocatalytic material because it work in the visible range of solar radiation.

Among the various structures and phases of iron oxides, the study of the photocatalytic activity of mesoporous iron oxide with metastable modification, like maghemite (γ -Fe₂O₃) are very interesting scientific task. Because in most cases increase the surface area of materials or the formation of porous structures with desired properties are important for applications. The mesoporous γ -Fe₂O₃ nanostructures, which gas process the combined advantages of rapid charge transfer pathway for carrier collection, large surface area for increased reaction sites, and excellent light trapping which are all favorable characteristics for photocatalytic reactions. As follows, the investigation of nanodispersed iron oxide crystal, formation of magnetic microstructure and the effect of synthesis conditions onto the materials phase composition and morphology are important and actual.

The formation of the mesoporous structure occurs as a result of the loss of physically adsorbed water and citrate groups, which ends at a temperature of about 330°C [5]. Dehydration and decomposition of oxyhydrochlorides occur in the temperature range 170-400°C. The interaction of surface groups >Fe - OH <leads to the appearance of interparticle bridges >Fe-O-Fe<. Given the defect and disorientation of the particles of the new phase, oxobridges between them will initiate recrystallization and partial agglomeration.

In this work, we have demonstrated a simple, reproducible and environmentally friendly method for the synthesis of nanostructured mesoporous γ -Fe₂O₃. The main aim of article are to investigate the influence of synthesis conditions, in particular the molarity of precursors, into the morphology, structure, optical, electrical conductivity and photocatalytic properties of γ -Fe₂O₃.

I. Materials and methods

Materials

Nanostructured γ -Fe₂O₃ obtained by the sol-gel route [6]. The first stage include the slowly mixing of aqueous solutions Fe(NO₃)₃·9H₂O and C₆H₈O₇·H₂O (molar concentrations 0.025M, 0.1M, 0.3M, 0.5M) and the next aging of obtained sol at 60°C on the air during about 6 days to formation of the iron citrate hydrate xerogels. The following, iron citrate xerogel were anneal at 175°C during 2 hour on the air. Obtained materials were marked accordingly to precursors molar concentrations.

Methods

The crystalline structure of the powder mixture studied by DRON-4-07 diffractometer with monochromatic Cu K α radiation (40 kV, 30 mA). Bragg-Brentano geometry and a Ni K β -filter were used. A qualitative analysis through ICSD structure models was carried out. FWHM for a diffraction peak of this reference sample at $2\theta = 43.38^\circ$ was 0.129° . The size of the coherently scattering domains calculated by the Scherrer equation:

$$D = \frac{K\lambda}{\beta \cos \theta}, \quad (1)$$

where K is the Scherrer constant ($K = 0.9$), λ is the wavelength (0.15405 nm), β the FWHM (in radians) and θ is the peak angular position. As profile shape, we used a combination of Gauss and Cauchy (dominated) functions.

The XPS core-level and valence-band spectra was recorded in an ion-pump chamber (base pressure less than 5×10^{-10} mbar) of the UHV-Analysis-System produced by SPECS Surface Nano Analysis Company (Berlin, Germany). In the System, a PHOIBOS 150 hemispherical analyzer were used. The XPS spectra of the γ -Fe₂O₃ samples were excited by the Mg K α source of X-ray radiation ($E = 1253.6$ eV) and were measured at constant pass energy of 25 eV. The spectrometer energy scale was calibrated by setting the Au 4f_{7/2} and the Cu 2p_{3/2} binding energies of pure metallic reference samples to 84.00 ± 0.05 eV and 932.66 ± 0.05 eV, respectively, in reference to the Fermi energy (E_F) [7]. The surface charging effects were accounted for by measuring the 1s line of adventitious carbon (284.6 eV) as suggested for iron- and oxygen-bearing compounds [8].

The morphology of the samples was studied by scanning electron microscopy (SEM) JSM- 6490 LV JEOL operated at 30 kV.

Electrical conductivity σ as a function of frequency was measured by the method of impedance spectroscopy in the frequency range of 0.01 - 100 kHz (Autolab PG-STAT 12/FRA-2 analyser); all samples were made in pellet form with the diameter of $17 \cdot 10^{-3}$ m and thickness of $0.1 \cdot 10^{-3}$ m under pressure about 33 - 35 MPa and the room temperature.

The optical transmittance spectra of samples were take by UV-VIS Spectrophotometer USB 2000 Fiber Optic Spectrometer in the wavelength range 400-900 nm.

Methylene blue (MB) used as a model to evaluate the photocatalytic activity of γ - chosen using the linear part of the absorbance-concentration curve. Visible light irradiation provided by a 500 W halogen lamp. To avoid the heating of the solutions were used the Corning K-glass filter. The residual concentration of MB solution were monitored using UV-visible absorption spectrometry ULAB-103 UV/VIS.

II. Results and discussion

X-ray diffraction analysis

According to XRD all materials obtained by thermal decomposition of xerogel are monophase ultrafine γ -Fe₂O₃ (Fig. 1). Average sizes of X-ray coherent scattering areas have tendency to growth with the precursors molar concentration increasing: 6 ± 2 for 0.025M and 0.1M samples, 7 ± 2 for 0.3M and 10 ± 2 nm for 0.5M.

X-ray diffraction analysis

Fig. 2 shows the survey XPS spectra of the γ -Fe₂O₃ samples obtained at different precursor molar concentrations. All XPS spectral features, except the C1s level and C KLL Auger line are account for the constituent atom core-levels or Auger lines of γ -Fe₂O₃.

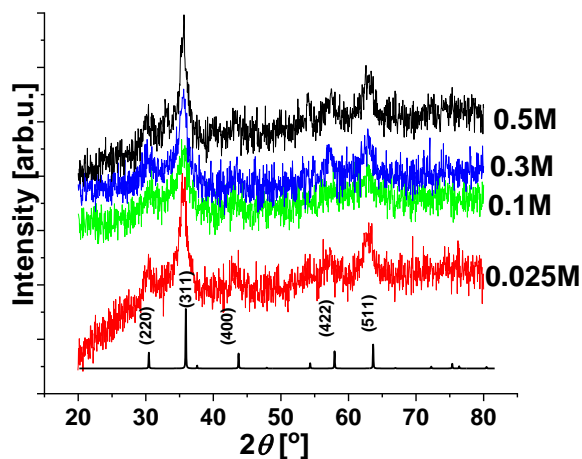


Fig. 1. XRD patterns of γ -Fe₂O₃ samples obtained at the different precursors molar concentration.

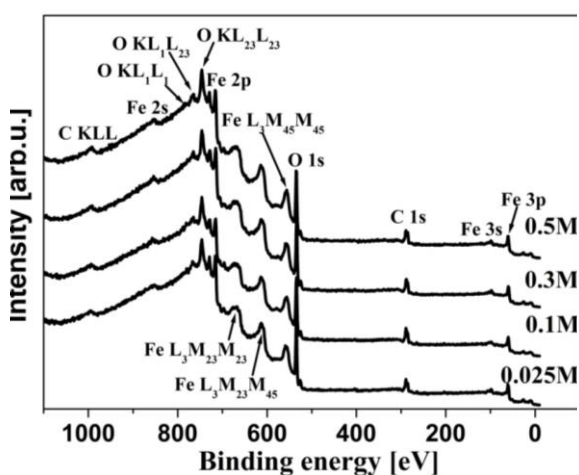


Fig. 2. Survey XPS spectra of γ -Fe₂O₃ samples obtained at different precursor molar concentrations.

Fig. 3 shows the main core-level spectra associated with iron and oxygen. The maxima of the XPS O 1s core-level spectra (Fig. 3, a) are positioned at about 530.0 ± 0.2 eV. This binding energy value corresponds to oxygen forming Fe–O bonds in γ -Fe₂O₃. However, all the O 1s core-level spectra characterize by the presence of a shoulder at about 531.8 eV.

The shoulder formed by oxygen-containing species adsorbed on the γ -Fe₂O₃ sample surfaces. XPS Fe 2p core-level spectra (Fig. 3, b) are simple spin doublets with the XPS Fe 2p_{3/2} binding energies $(710.9 - 711.0) \pm 0.1$ eV corresponding to iron atoms in charge state Fe³⁺ [9]. We did not detect any visible changes in shapes and energy positions of the maxima of the XPS Fe 2p core-level spectra with changes in precursor molar concentrations of the γ -Fe₂O₃ samples under consideration. However, from Fig. 3, c, we could see some changes in the XPS C 1s core-level spectra. From this figure, we can see that the C 1s spectra reveal a three-peak structure in every studied sample. The main peak at 284.6 eV obviously attributed to adventitious hydro-

carbons, while the shoulder at about 288 eV could be explain by the presence of C–NH_x groups adsorbed on the sample surfaces [10].

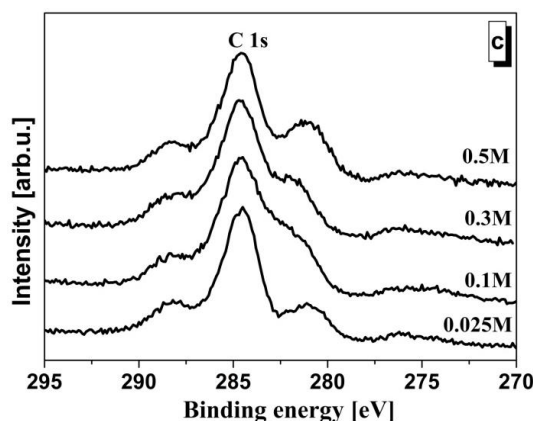
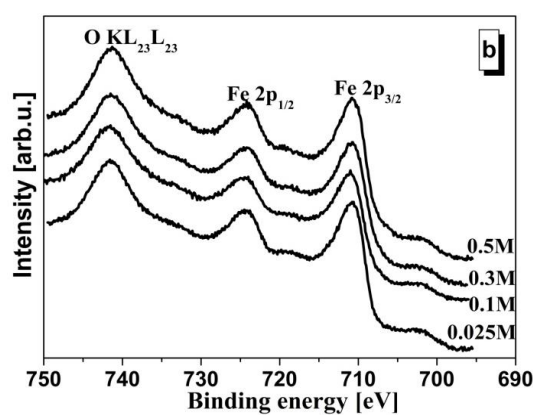
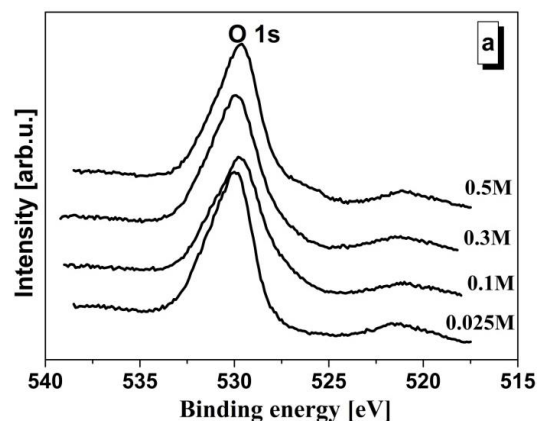


Fig. 3. XPS (a) O 1s, (b) Fe 2p and (c) C 1s core-level spectra of γ -Fe₂O₃ samples obtained at different precursor molar concentrations.

The origin of the fine-structure peculiarity at 281 - 282 eV of the XPS C 1s core-level spectra measured for γ -Fe₂O₃ obtained at different precursor molar concentrations is probably due to formation of some carbon bonding with iron in the superficial layers of the particle. However, this suggestion needs additional studies for clarifying the origin of the mentioned fine-structure peculiarity of the measured C 1s core-level spectra.

The XPS valence-band spectra presented in Fig. 4

reveal no visible alterations in their shapes and energy positions of the fine-structure peculiarities when changing molar concentrations during synthesis of the γ - Fe_2O_3 samples under study.

Impedance spectroscopy analysis

Fig. 5 shows the frequency dependences of the conductivity γ - Fe_2O_3 samples obtained at the different precursors molar concentration. Curves have peculiarities typical for disordered dielectrics and semiconductors – weak changes of the conductivity at low frequencies and

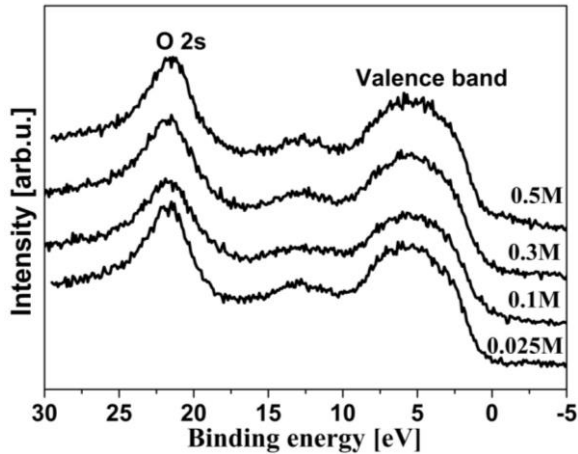


Fig. 4. XPS valence-band spectra (including upper O 2s core-level) of γ - Fe_2O_3 samples obtained at different precursor molar concentrations.

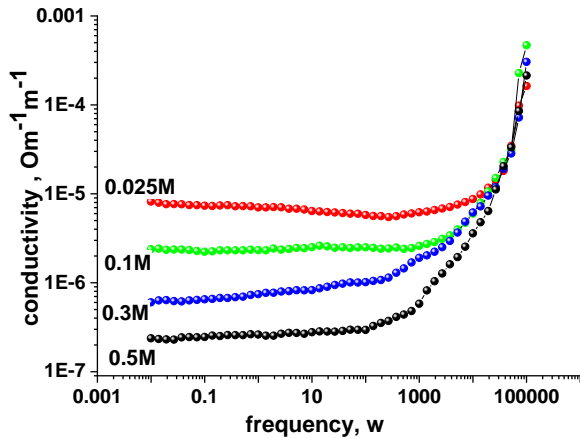


Fig. 5. The frequency dependence of the real conductivity $\sigma(\omega)$ for γ - Fe_2O_3 samples obtained at different precursors molar concentrations (The solid lines are obtained from a Jonscher power-law fit of ac conductivities).

the increase with frequency enlarging. For interpretation of electrical-relaxation phenomena for dc and ac conductivities, Jonscher power law were used:

$$\sigma(\omega) = \sigma_{dc} \left[1 + \left(\omega / \omega_h \right)^s \right]^{-1}, \quad (2)$$

where σ_{dc} is the dc conductivity, ω_h is the hopping frequency of the charge carriers, and s is a frequency exponent parameter in the range $0 < s < 1$ characterizing the deviation from Debye behavior and measurement of

the interionic coupling strength [11].

For 0.1 M and 0.5 M $s = 0.94$ and 0.98 , respectively and this indicates that these system is in a state close to the Debye model and observed conductivity behavior can explained by small polaron hopping mechanism [12]. The electrical properties of maghemite as wide-band semiconductor materials was caused by short-range metal-ligand bonding. According to calculations [13], conduction states of iron oxides are highly localized and strong electron-phonon interactions stabilize charge carriers in a lattice distortion, forming midgap polaronic states. As a result, electrons localized at partially filled $3d$ -states will self-localize as metal-centered small polarons. In our case, correlated barrier hopping [14] is the most appropriate model. The power law exponents (s) lies between 1 and 0.5 in the case of long-range pathways and diffusion-limited hopping. The increase in ac conductivity would be attribute to the lowering of the activation barrier at higher frequencies. For another two samples (0.025 M and 0.3 M) power law exponents are grater then 0.6 (0.75 and 0.85, respectively) and as a result they have the same conductivity mechanism with the morphological peculiarities influence.

The dc conductivity (σ_{dc}) decrease with the increasing of molar concentration, which was caused by the enlarging of average size of primary particles (Fig. 5) (corresponds to the sizes of X-ray coherent scattering areas). These data is an indirect confirmation of XRD patterns interpretation. In addition, the crystal structures of maghemite and magnetite are very close and these phases XRD separation for the case of disordered samples is the complex task. The specific conductivity of magnetite is about $10^2 - 10^3 \text{Om}^{-1}\text{cm}^{-1}$, while for maghemite this characteristic is 8 - 9 orders lower [15].

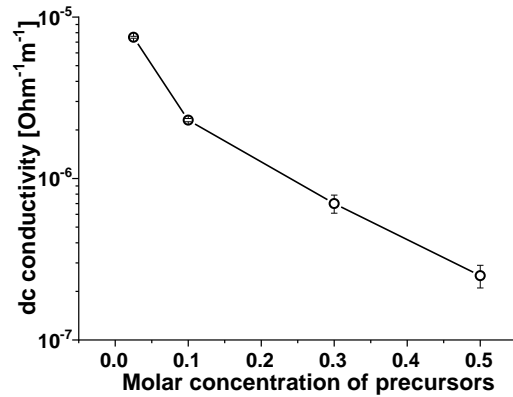


Fig. 6. The depending of dc conductivity and charge carriers hopping frequency of γ - Fe_2O_3 samples vs different molar concentration of precursors.

Fig. 6 shows changing of dc conductivity and charge carriers hopping frequency of γ - Fe_2O_3 samples vs different molar concentration of precursors. From these curve we could see, law charge carriers hopping frequency have the local maximum for the 0.1 M sample with the continuous decrease with the next particle size enlarging for materials.

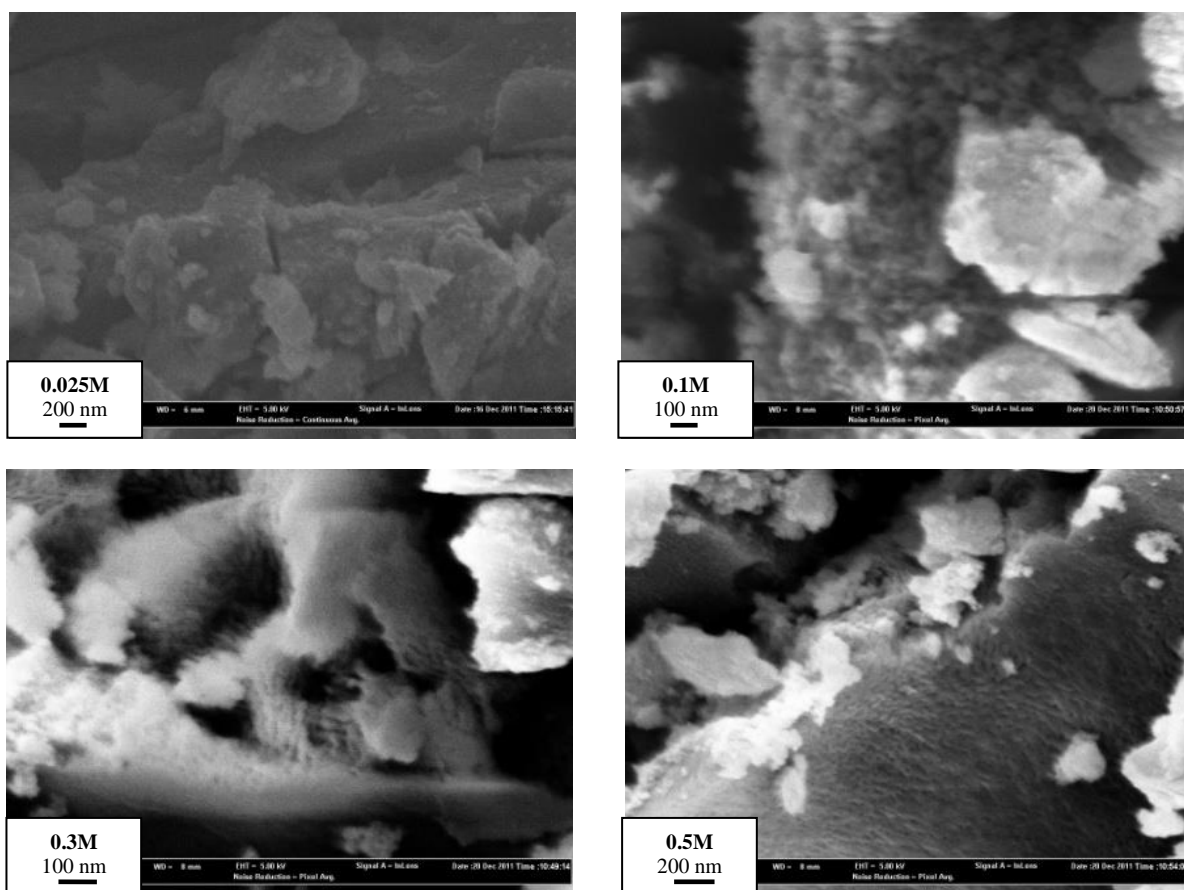


Fig. 7. SEM images of γ -Fe₂O₃ samples obtained at different precursors molar concentrations.

SEM study

Accordingly to the SEM data, all obtained materials are characterized by porous structure as a result of evaporation of metal-organic precursor decomposition products at the initial xerogel thermal treatment (Fig. 7).

The tendency to porosity increasing with the enlarging of precursors molar concentration was observed for 0.025 M, 0.1 M and 0.3 M samples. At the same time, large agglomerates and cracks present on the sponge-like porous surface of 0.5 M material.

Morphological study

Isotherms of adsorption/desorption for the all samples have hysteresis of H4 which is characteristic of mesoporous materials with pore diameter of 2 - 50 nm. Specific surface areas of obtained materials vary depending on the precursors molar concentrations in a range 105 - 160 m²/g (Fig. 8).

The increasing of precursors concentration up to 0.3 M causes the porosity increase that agrees with the SEM results. The decreasing of specific surface area for

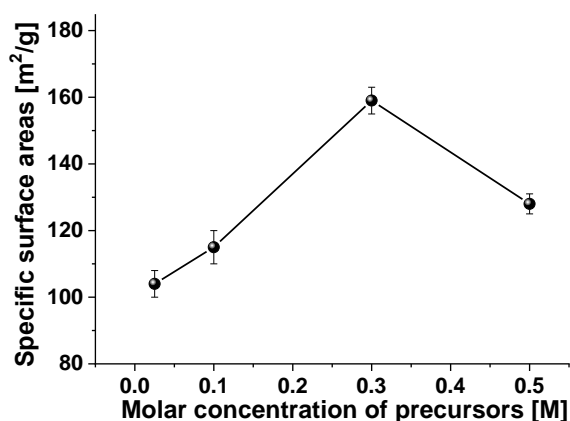


Fig. 8. Specific surface area of γ -Fe₂O₃ samples obtained at different precursors molar concentrations.

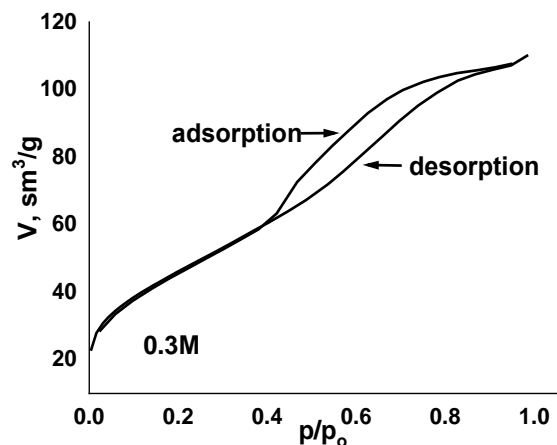


Fig. 9. Adsorption-desorption isotherms samples of series 0.3 M.

0.5 M sample corresponds to particles enlarging. The maximum for 0.3 M sample are the result of develop porous structure (Fig. 9).

For all samples there is a characteristic the dependence of the specific volume of pores on size in the range of 3 - 7 nm and the presence of a maximum around 5 nm. For 0.3 M series samples, in addition to the generally higher value of the pore volume, mesopores with a diameter of 2 - 3 nm has present. We can also identify pores with a size of about 4 nm, the relative concentration of which varies for different sample systems. Increasing the value of the specific surface area of the samples of series 0.3 M leads to an increase in the pore volume: for the sample annealed at 175 °C the pore volume is 0.165 cm³/g (Fig. 9), while for the sample series 0.5 M annealed at the same temperature - 0.140 cm³/g.

Band gap study

Another proof of nanodispersed maghemite obtaining are optical absorption data (Fig. 10, a). For all materials, bandgap energy is close to 2.0 eV that corresponds to γ -Fe₂O₃ [16], while for Fe₃O₄ bandgap energy is about 0.1 eV [17]. Bandgap of obtained materials are investigations by used optical spectroscopy in the visible ranges. The optical transmittance spectra of the synthesized materials (water dispersions) studied in

the range 400 - 900 nm.

The nature of the transitions and the band gap calculated by using equation:

$$\alpha = \text{const}/h\nu \cdot [h\nu - E_g]^{1/2}, \quad (3)$$

where $n = 1/2$ for direct optical transitions and $n = 2$ for indirect transitions. The plots of $(\alpha h\nu)^2$ as a function $h\nu$ (Fig. 10, b) have a linear character, so all obtained material have direct optical band gap. The extrapolation of the straight line to a $\alpha = 0$ gives a direct band gap values. These values decreased from 2.18 to 2.04 eV with increase in molarity of the precursor sol from 0.025 to 0.5 M.

On the other hand, we can see a clear correlation: with increasing dispersion of the material and decreasing particle size, the size of the band gap increases.

At [18] proposed the correlation model between the effective band gap of a material and the average particle size based on the variation of exciton energy and particle size. The ground state of the electron hole pair are the lowest excited state of the crystallite.

The ground state energy of an exciton or the increase in effective band gap as a function of crystalline size estimated as:

$$E_g(R) = E_g^{\text{Bulk}} + h^2/8R^2 \cdot [1/m_e^* + 1/m_p^*] - 1.8e^2/4\pi\epsilon\epsilon_0R, \quad (4)$$

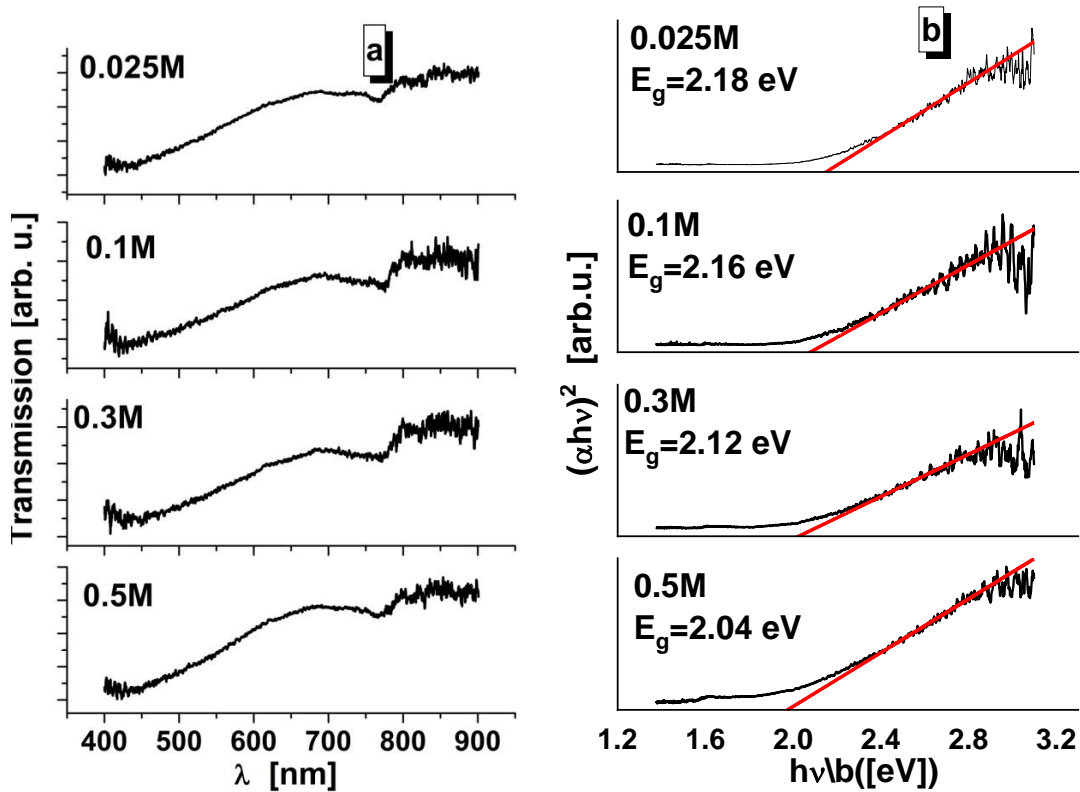


Fig. 10. Transmission spectra (a) and dependence $[\alpha h\nu]^2(h\nu)$ (b) for γ -Fe₂O₃ samples obtained at different precursors molar concentrations.

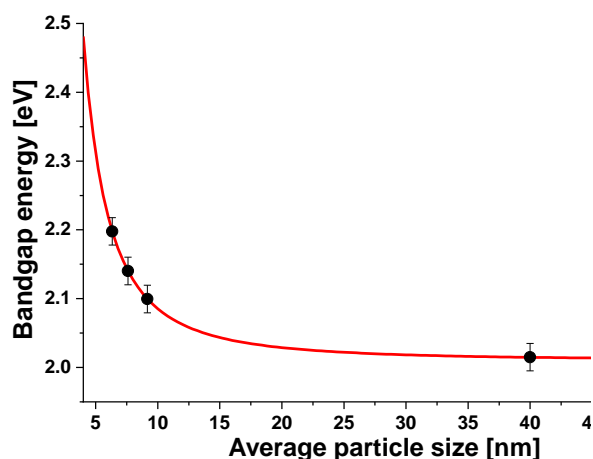


Fig. 11. Calculated using Brus equation size-dependent bandgap energy for γ -Fe₂O₃ (solid line) and overlaid experimental bandgap energies values for optical direct transitions (dots).

where $E_g(r)$ is the band gap of the nanoparticle, E_g^{bulk} is the bulk semiconductor band gap, h is Planck's constant (6.6260×10^{-34} m² kg/s), ϵ is the relative dielectric constant of the material [19], ϵ_0 is the permittivity of free space, R is the radius of the particle, m_e and m_h is the effective masses of the electron and hole.

Thus, analyzing equation (4), we can say that when the linear size of particles decreases, the width of the band gap of the material increases. Fitted by Brus equation proposed the dependence of the band gap blue shift on the average particle size of synthesized maghemite and bulk material (Fig. 11).

It was found that for all synthesized samples of maghemite, the band gap is higher than for bulk material. In this case, the increasing of band gap compared to bulk γ -Fe₂O₃ caused by quantum confinement. The insignificant increasing of band gap of all materials can be connected from the dispersion of material after sintering at 175 °C and the reconstruction effects of γ -Fe₂O₃ nanoparticles surface.

Photocatalytic degradation study

Photocatalytic activity of synthesized materials were appreciated as degradation profile of MB and formaldehyde in water under the illumination of UV and visible light. The initial degradation rates of reaction are determined by conducting a series of concentration versus time experiments. The photocatalytic degradation of MB dye shows in (Fig. 12, a).

The highest photocatalytic activity is characteristic of the 0.3 M sample. This material, the fastest destroys the dye MB. For all other samples, the destruction time of the dye is the same. The calculated values of the destruction rate and the constructed dependence on the molar concentration of precursors are presented in Fig. 12, b. As can be seen from the Fig. 12, b and taking into account Fig. 8 it can be argued that the photo activity of the materials depends on the specific surface area. There is a clear correlation – the more dispersed of material, so the better its photo activity.

It known, that the morphology of mesoporous maghemite depends on the molar concentration of precursors [20] – the increase in the molar concentration of precursors leads to an increase in the particle size of the maghemite. As a result of annealing of iron citrate, there is competition between two processes: dispersion of the material due to gas evolution and combustion of the organic component and sintering of material particles. In turn, at higher molarities of the initial solution and sintering and aggregation of particles predominate over the processes of dispersion, which leads to the formation of particles of larger material [21]. Since the photocatalytic activity of the material depends on the surface reactions dye to destruction, the material with a larger specific surface area will have the highest photocatalytic activity. This conclusion confirms by the construction of the dependence of the rate of photo degradation of the dye on the molar concentration of the original precursor. Nano dispersed mesoporous γ -Fe₂O₃ obtained from 0.3 M solution of iron citrate is the best photo catalyst for the destruction of organic pollutants.

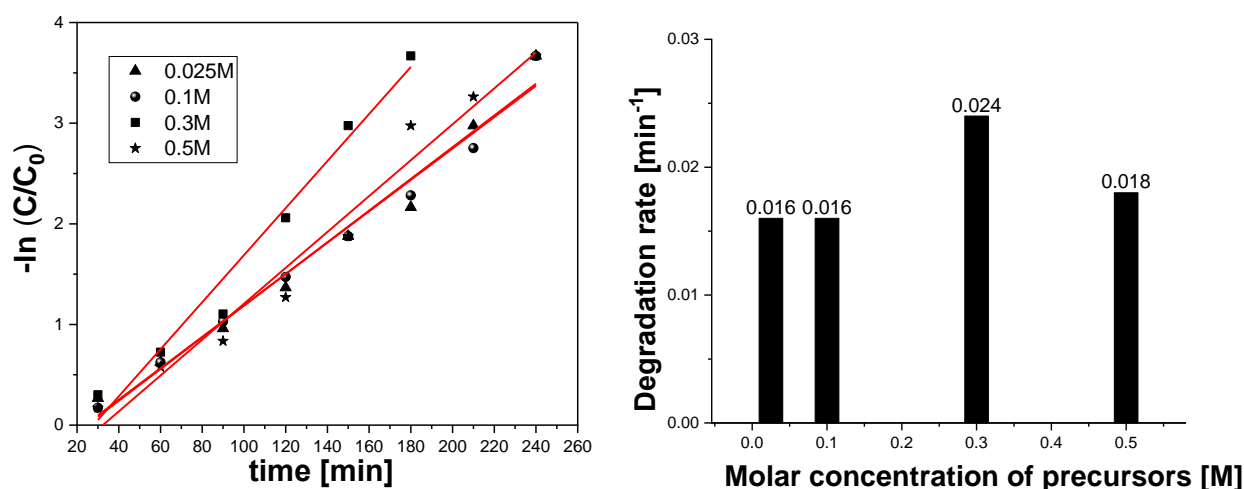


Fig. 12. The photocatalytic degradation of MB dye (a) and destruction rate dependence on the molar concentration of precursors (b).

Conclusions

The sol-gel approach of nanostructured γ -Fe₂O₃ synthesis with different precursor's molarity, which has permitted to obtain the materials with mesoporous structure was proposed. The XPS valence-band spectra reveal no visible alterations in their shapes and energy positions of the fine-structure peculiarities when changing molar concentrations during synthesis of the γ -Fe₂O₃ samples under study. The average particle sizes, specific surface area, pore sizes distributions, optical and conductivity properties depended on precursor's molarity were investigated. The mechanism of electrical conductivity formation for synthesized mesoporous materials was established. The correlation between photo degradation constant rates and specific surface area and band gap were determined. The increasing of specific

surface area causes the growth of photo activity of materials.

Hrubciak A.B. – PhD, doctoral student;
Khyzhun O.Yu. – Doctor of Physical and Mathematical Sciences, Senior Scientist;
Ostafiychuk B.K. – Professor, Doctor of Physical and Mathematical Sciences, Corresponding Member of NAS of Ukraine;
Moklyak V.V. – Doctor of Physical and Mathematical Sciences, Senior Scientist;
Yavorskyi Yu.V. – PhD, Researcher/Assistant;
Lisovsky R.P. – Doctor of Physical and Mathematical Sciences, Senior Specialist of Joint educational and scientific laboratory "Physics of Magnetic Films";
Keush L.G. – PhD, doctoral student;
Onyskiv B.B. – Master of Physical, expert.

- [1] S.W. Cao, Y.J. Zhu, M.Y. Ma, L. Li, L. Zhang, J. Phys. Chem. C. 112(6), 1851 (2008) (DOI: [10.1021/jp077468+](https://doi.org/10.1021/jp077468+)).
- [2] M. Levy, C. Wilhelm, J.M. Siaugue, O. Horner, J.C. Bacri, F. Gazeau, J. Phys. Condens. Matter. 20(6), 204133 (2008) (DOI: [10.1088/0953-8984/20/20/204133](https://doi.org/10.1088/0953-8984/20/20/204133)).
- [3] S. Capone, M.G. Manera, A. Taurino, P. Siciliano, R. Rella, S. Luby, E. Majkova, Langmuir. 30(4), 1190 (2014) (DOI: [10.1021/la404542u](https://doi.org/10.1021/la404542u)).
- [4] Yu.V. Yavorskyi, Ya.V. Zaulychnyy, M.V. Karpets, A.B. Hrubciak, V.V. Moklyak, O.I. Dudka, Ya.A. Kononenko, Physics and Chemistry of Solid State 20(4), 360 (2019) (DOI: [10.15330/pcss.20.4.360-366](https://doi.org/10.15330/pcss.20.4.360-366)).
- [5] E. Darezereshki, Materials Letters, 65, 642 (2011) (DOI: [10.1016/j.matlet.2010.11.030](https://doi.org/10.1016/j.matlet.2010.11.030)).
- [6] V. Kotsyubynsky, A. Grubiak, V. Moklyak, V. Pylypiv, R. Lisovsky, Metallofizika i Noveishie Tekhnologii. 36, No 11, 1497 (2014) (DOI: [10.15407/mfint.36.11.1497](https://doi.org/10.15407/mfint.36.11.1497)).
- [7] O.Y. Khyzhun, V.L. Bekenev, V.V. Atuchin, E.N. Galashov, V.N. Shlegel, Mater. Chem. Phys. 140(2-3), 588 (2013) (DOI: [10.1016/j.matchemphys.2013.04.010](https://doi.org/10.1016/j.matchemphys.2013.04.010)).
- [8] S. Rajagopal, D. Nataraj, O.Y. Khyzhun, Y. Djaoued, J. Robichaud, D. Mangalaraj, J. Alloys. Compd. 493(1-2), 340 (2010) (DOI: [10.1016/j.jallcom.2009.12.099](https://doi.org/10.1016/j.jallcom.2009.12.099)).
- [9] D. Briggs, P.M. Seach, Practical Surface Analysis (2nd Ed.): Auger and X-Ray Photoelectron Spectroscopy (Chichester, John Wiley & Sons Ltd, 1990).
- [10] T.I.T. Okpalugo, P. Papakonstantinou, H. Murphy, J. McLaughlin, N.M.D. Brown, Carbon. 43(1), 153 (2005) (DOI: [10.1016/j.carbon.2004.08.033](https://doi.org/10.1016/j.carbon.2004.08.033)).
- [11] A.K. Jonscher, Universal Relaxation Law (London: Chelsea Dielectrics Press, UK, 1996).
- [12] N.F. Mott, J. Non-Cryst. Solids. 1(1), 1 (1968) (DOI: [10.1016/0022-3093\(68\)90002-1](https://doi.org/10.1016/0022-3093(68)90002-1)).
- [13] K.M. Rosso, M. Dupuis, J. Chem. Phys. 120(15), 7050 (2004) (DOI: [10.1063/1.1676117](https://doi.org/10.1063/1.1676117)).
- [14] S.R. Elliott, Philos. Mag. 36(6), 1291 (1977) (DOI: [10.1080/14786437708238517](https://doi.org/10.1080/14786437708238517)).
- [15] R.M. Cornell, U. Schwertmann, The Iron Oxides: Structure, Properties, Reactions, Occurrences and Uses (Weinheim, Wiley-VCH Verlag GmbH & Co, 2003).
- [16] A. Cabot, V.F. Puentes, E. Shevchenko, Y. Yin, L. Balcells, M.A. Marcus, S.M. Hughes, A.P. Alivisatos, J. Am. Chem. Soc. 129(34), 10358 (2007) (DOI: [10.1021/ja072574a](https://doi.org/10.1021/ja072574a)).
- [17] K.S. Jung, K.W. Sung, Magnetite: Electrochemical Properties And Its Role On Flow Accelerated Corrosion, Magnetite: Structure, Properties and Applications (Nova Science Publishers, New York, 2010).
- [18] L.E. Brus, J. Chem. Phys. 79(11), 5566 (1983) (DOI: [10.1063/1.445676](https://doi.org/10.1063/1.445676)).
- [19] T.D. Glotch, G.R. Rossman, Icarus. 204(2), 663 (2009) (DOI: [10.1016/j.icarus.2009.07.024](https://doi.org/10.1016/j.icarus.2009.07.024)).
- [20] V. Kotsyubynsky, B. Ostafiychuk, V. Moklyak, A. Hrubciak, Solid State Phenomena. 230, 120 (2015) (DOI: [10.4028/www.scientific.net/SSP.230.120](https://doi.org/10.4028/www.scientific.net/SSP.230.120)).
- [21] L. Kieush, M. Boyko, A. Koveria, A. Khudyakov, A. Ruban, Eastern-European Journal of Enterprise Technologies 1(6), 34 (2019) (DOI: [10.15587/1729-4061.2019.154082](https://doi.org/10.15587/1729-4061.2019.154082)).

А.Б. Груб'як¹, О.Ю. Хижун², Б.К. Остафійчук^{1,3}, В.В. Мокляк^{1,3}, Ю.В. Яворський⁴,
Р.П. Лісовський^{1,3,5}, Л.Г. Кеуш⁶, Б.Б. Ониськів⁷

Наноструктурований мезопористий γ -Fe₂O₃ як новий фотокаталізатор для деградації органічних забруднювачів

¹Інститут металофізики ім. Г.В. Курдюмова НАН України, Київ, Україна, hrubyak_andrii@ukr.net

²Інститут матеріалознавства імені І.М. Францевича НАН України, Київ, Україна, khyzhun@ukr.net

³ДВНЗ "Прикарпатський національний університет імені Василя Стефаника",

Івано-Франківськ, Україна hrubyak_andrii@ukr.net

⁴Національний технічний університет України "Київський політехнічний інститут імені Ігора Сікорського",

Київ, Україна, yar-vra@ukr.net

⁵Івано-Франківський національний медичний університет, Івано-Франківськ, Україна, lesrom2000@gmail.com

⁶Національна металургійна академія України, Дніпро, Україна, linakeush@gmail.com

⁷Івано-Франківський науково-дослідний криміналістичний центр МВС України,

Івано-Франківськ, Україна, onuskivb@gmail.com

Модифікований метод синтезу золь-гель був використаний для створення наноструктурованого магеміту (γ -Fe₂O₃). Показано, що молярна концентрація прекурсорів під час синтезу впливає на структурно-морфологічні, оптичні та провідні властивості отриманих матеріалів. Метод XPS дозволив встановити особливості електронної структури синтезованих матеріалів. Вибрано оптимальні умови синтезу наноструктурованого магеміту з мезопористою структурою. Встановлено механізм формування електропровідності для синтезованих мезопористих матеріалів. Визначено ширину забороненої зони та встановлено її залежність від молярної концентрації прекурсорів. Встановлено позитивну кореляцію між питомою поверхнею зразків γ -Fe₂O₃ та фотокаталітичною активністю - фотокаталітична активність синтезованих зразків γ -Fe₂O₃ зростає із збільшенням питомої поверхні.

Ключові слова: наноструктурований магеміт, мезопориста структура, електропровідність, питома площа поверхні, ширина забороненої зони, фотокаталіз.